WILEY-BLACKWELL

Biotechnology and Applied Biochemistry

Clickable artificial heme-peroxidases for the development of functional nanomaterials

Journal:	*Biotechnology and Applied Biochemistry*
Manuscript ID	Draft
Wiley - Manuscript type:	Original Article
Date Submitted by the Author:	n/a
Complete List of Authors:	Zambrano , Gerardo; University of Naples Federico II, Department of Chemical Sciences Chino, Marco; University of Naples Federico II, Department of Chemical Sciences Renzi, Emilia; University of Naples Federico II, Department of Chemical Sciences Di Girolamo , Rocco; University of Naples Federico II, Department of Chemical Sciences Maglio, Ornella; University of Naples Federico II, Department of Chemical Sciences; Istituto di Biostrutture e Bioimmagini Consiglio Nazionale delle Ricerche Pavone, Vincenzo; University of Naples Federico II, Department of Chemical Sciences Lombardi, Angela; University of Naples Federico II, Department of Chemical Sciences Nastri, Flavia; University of Naples Federico II, Department of Chemical Sciences
Keywords:	click chemistry; gold nanoparticles; metalloenzymes; miniaturization; peroxidases; protein design
Mandatory Keywords:	Biocatalysis, Immobilization, Nanoparticle, Nanomaterials, Enzyme
Abstract:	Artificial metalloenzymes as catalysts are promising candidates for their use in different technologies, such as bioremediation, biomass transformation or biosensing. Despite this, their practical exploitation is still at an early stage. Immobilized natural enzymes have been proposed to enhance their applicability. Immobilization may offer several advantages: i) catalyst re-use; ii) easy separation of the enzyme from the reaction medium; iii) better tolerance to harsh temperature and pH conditions. Here, we report an easy immobilization procedure of an artificial peroxidase on different surfaces, by means of click chemistry. FeMC6*a, a recently developed peroxidase mimic, has been functionalized with a pegylated aza-dibenzocyclooctyne to afford a "clickable" biocatalyst, namely FeMC6*a-PEG_4@DBCO, which easily reacts with azide-functionalized molecules and/or nanomaterials to afford functional bioconjugates. The clicked biocatalyst retains its structural and, to some extent, its functional behaviors, thus housing high potential for biotechnological applications.

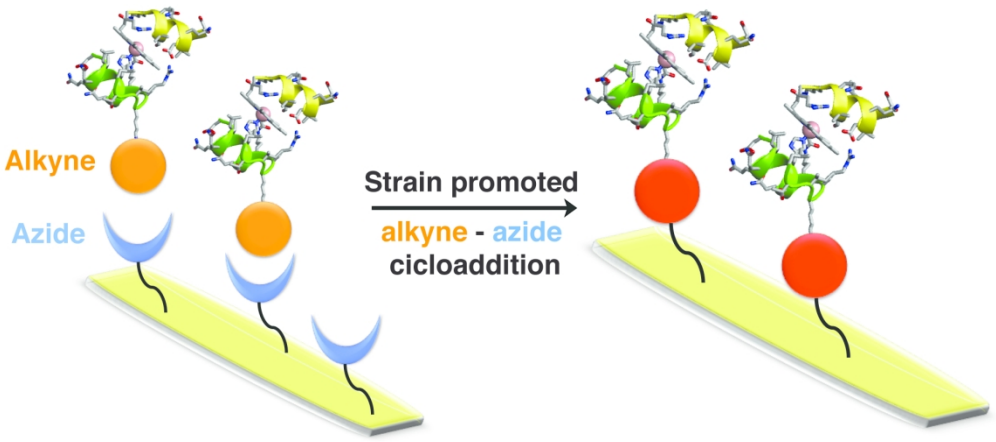

Clickable artificial peroxidase for fast and selective modification of surfaces and nanomaterials

Clickable artificial heme-peroxidases for the development of functional nanomaterials

by

Gerardo Zambrano[1], Marco Chino[1], Emilia Renzi[1], Rocco Di Girolamo[1], Ornella Maglio[1,2], Vincenzo Pavone[1], Angela Lombardi[1]* and Flavia Nastri[1]*

[1]Department of Chemical Sciences, University of Napoli "Federico II" Via Cintia, 80126 Napoli, Italy;

[2]Istituto di Biostrutture e Bioimmagini, CNR, Via Mezzocannone 16, 80134 Napoli, Italy;

Corresponding authors

*Flavia Nastri

e-mail: flavia.nastri@unina.it

Phone number: +39081674419

Fax number: +39081674090

*Angela Lombardi

e-mail: angela.lombardi@unina.it

Phone number: +39081674418

Fax number: +39081674090

Running title *Clickable artificial heme-peroxidases*

Synopsis

Artificial metalloenzymes as catalysts are promising candidates for their use in different technologies, such as bioremediation, biomass transformation or biosensing. Despite this, their practical exploitation is still at an early stage. Immobilized natural enzymes have been proposed to enhance their applicability. Immobilization may offer several advantages: *i)* catalyst re-use; *ii)* easy separation of the enzyme from the reaction medium; *iii)* better tolerance to harsh temperature and pH conditions. Here, we report an easy immobilization procedure of an artificial peroxidase on different surfaces, by means of click chemistry. FeMC6*a, a recently developed peroxidase mimic, has been functionalized with a pegylated aza-dibenzocyclooctyne to afford a "clickable" biocatalyst, namely FeMC6*a-PEG_4@DBCO, which easily reacts with azide-functionalized molecules and/or nanomaterials to afford functional bioconjugates. The clicked biocatalyst retains its structural and, to some extent, its functional behaviors, thus housing high potential for biotechnological applications.

Keywords (up to six in alphabetical order): click chemistry; gold nanoparticles; metalloenzymes; miniaturization; peroxidases; protein design.

Abbreviations: MCs, Mimochromes; SAM, self-assembled monolayer; ITO, tin-doped indium oxide; LA, lipoic acid; AuNPs, gold nanoparticles; Cu-AAC, copper-catalyzed alkyne-azide cycloaddition; SPAAC, strain promoted azide-alkyne cycloaddition; PEG, polyethylene glycol; DBCO, aza-dibenzocyclooctyne; NHS, N-hydroxysuccinimide; MTBE, methyl-*tert*-butyl ether; LA@N_3, 3-azidopropyl-5-(1,2-dithiolan-3-yl)pentanamide; SPRB, surface plasmon resonance band; TFA, trifluoroacetic acid; DMF, dimethylformamide; TFE, 2,2,2-trifluoroethanol; HATU 1-[bis(dimethylamino)methylene]-1H-1,2,3-triazole[4,5-b]pyridinium 3-oxid hexafluorophosphate; ABTS, 2,2'-azino-bis (3-ethylbenzothiazoline-6-sulphonic acid); DIEA, *N*,*N*-diisopropylethylamine; Aib, 2-amino isobutyric acid; DMSO, dimethylsulfoxide; PPh_3, triphenylposphyine; AcOEt, ethyl acetate; Et_2O, diethyl ether; DCM, methylene chloride; R_G, radius of gyration.

1. Introduction

The field of metalloenzyme design and engineering is approaching its "golden age". By using several tools and complementary strategies, protein designers are capable of implanting a variety of functions into native or designed protein scaffolds [1-6]. The research field now appears to have limitless potential, as protein scaffolds can be shaped, optimized or repurposed to obtain artificial catalysts highly competent toward specific functions. Indeed, several outstanding examples demonstrate that it is possible to obtain artificial metalloenzymes behaving as oxydases, oxygenases and peroxidases [1,2, 7-13], hydrolases [1,2, 14-16] and hydrogenases [1-18]. The astonishing potential of this field has further been disclosed by the development of artificial metalloenzymes able to catalyze reactions with unknown natural counterparts [5, 19-23].

Along these lines, we have developed artificial metal-containing biocatalysts, named Mimochromes (MCs), by using a miniaturization process on hemeproteins [1, 10, 11, 24-33]. MCs consist of a helix-heme-helix sandwich, made up by two small peptide chains covalently linked to deuteroporphyrin. The helical peptide architecture around the porphyrin is able to fine modulate the catalytic behaviors of the metal ion inserted into the ring. Indeed, peroxidase activity was engineered and optimized into MC scaffold, by mimicking the first and second coordination spheres of natural heme-peroxidases. A tetradecapeptide (*TD*) chain bears the His axial proximal ligand and a decapeptide (*D*) chain, lacking the metal coordinating residue, resembles the distal site of heme-peroxidase for accommodating hydrogen peroxide. An iterative process of design and redesign afforded MC6*a [30] (Figure 1). Taking advantage of our knowledge in the use of non-proteogenic amino acids as conformational constraints to modulate peptide activity [34], we inserted two residues of 2-amino isobutyric acid (Aib) in the *(D)* chain, to reduce backbone flexibility, favor the helical folding, and stabilize the overall structural topology of MCs. This simple modification rendered MC6*a the most proficient and stable scaffold for modulating the reactivity of the porphyrin metal ion. MC6*a iron- and manganese- complexes were found to be competent catalysts in peroxidase and peroxygenase

activities [30, 31], respectively, whereas the cobalt derivative was active in hydrogen evolution catalysis [32, 33].

Despite significant achievements reached in the field of artificial metalloenzymes, practical applications in catalysis, biotechnology and sensor technology have scarcely been explored. Immobilization onto a support is a usual strategy for exploiting natural enzymes in industrial processes, as it allows enzyme reuse and separation from the reaction mixture [35-39]. Thus, evaluating the performances of artificial enzymes upon immobilization could be an important step toward their use in applicative process [40]. Moreover, the use of properly designed metalloenzymes, as substituted of natural enzymes in surface immobilization, would provide new possibility for the construction of catalytically active biomaterials, tailored for specific uses.

Enzymes can be immobilized on different surface mainly by means of covalent bond, entrapment or physical adsorption [35-39]. Selection of one of these strategies is not straightforward, as it is important to get stable metalloenzyme immobilization without damaging or losing its functional and conformational properties [35-39]. Proper immobilization strategy should be selected by evaluating several factors, such as: 1) the intended application the metalloenzyme should be used for; 2) the activity and stability of the enzyme upon immobilization; 3) the simplicity in preparation and handling; 4) the stability of the surface in the reaction media [41-44].

Within the efforts of exploiting our miniaturized heme-enzymes for practical applications, we have started investigating the behaviors of MCs upon immobilization onto different surfaces [45-47]. To this aim, we have evaluated two main strategies: physical adsorption and covalent binding. The first strategy revealed to be very useful to investigate MCs redox behaviors [45]. Hydrophobic interactions between the nonpolar patch of Fe(III)-MC6 and a self-assembled monolayer (SAM) of decane-1-thiol, coating a polycrystalline gold electrode, allowed proper immobilization of this catalyst. The immobilized Fe(III)-MC6 retained its redox properties and was able to catalytically reduce dioxygen, similarly to five-coordinate cytochrome c variants [45]. Changing the nature of the surface did not influenced the catalyst behaviors, as the redox properties of Fe(III)-MC6 were also retained upon

adsorption on mesoporous conductive films of tin-doped indium oxide (ITO) [46]. Further, as ITO is a solid support with high transparency in the visible spectrum, it allowed recording the UV-vis and resonance Raman spectra of the immobilized Fe(III)-MC6. All the data revealed that the immobilized complex behaves similarly to the freely diffusing in solution [27, 29].

Even though physical adsorption is simple and fast, it has also severe drawbacks, as enzymes tend to leach out from the surface. Indeed, reuse of the Fe(III)-MC6 functionalized gold electrode was limited by the natural loss of the immobilized enzyme from the adsorbed layer [45]. To solve this problem and develop biomaterials with applications in catalysis, we explored MCs catalytic behaviors upon covalent binding between the catalyst and the supporting material. Covalent immobilization minimizes the loss of enzyme from the surface, even upon changes of several factors, such as pH and presence of organic solvents [35, 36]. An important drawback of this method is the need of functionalizing the enzyme with linkers and reactive groups [35, 36], which may in principle cause enzyme denaturation and affect catalytic activity.

Recently, we developed a strategy based on the functionalization of a MC analogue with lipoic acid (LA) to construct a redox- and catalytically-active artificial enzyme, that could be easily and rapidly grafted onto different gold-based supports, such as electrodes and nanoparticles (AuNPs) [47]. In order to set up a general and broad strategy for the fast-covalent immobilization of MCs derivatives on various nanomaterials, we exploited the “click chemistry”. Click chemistry refers to a variety of reactions, widely used to join different chemical entities *via* heteroatom links. First introduced by Sharpless and coworkers [48], the click chemistry approach allows to rapidly and selectively link building blocks with different functionalities. Starting from the development of small molecules as drugs, the method has been extended to the world of biorthogonal chemical reactions, *i.e.* reactions working under physiological conditions to conjugate, label or modify life-sustaining macromolecules, as proteins, nucleic acids and antibodies [49]. The copper(I)-catalyzed alkyne-azide cycloaddition, also referred to as Cu-AAC, has become the prototypical click reaction [49, 50]. A more biocompatible version of this reaction is the strain promoted azide-alkyne cycloaddition reactions

(SPAAC), usually referred to as "copper-free click reaction" [51], which avoid the use of copper ions as catalyst, and rapidly proceeds to the desired product, thanks to the presence of strained alkynes, as cyclooctynes [52-54].

We previously exploited the modularity and efficiency of this class of reactions to afford the fast combination of two different peptide moieties thus generating a unique asymmetric artificial metalloenzymes [55, 56]. In this work, we report the functionalization of the miniaturized heme-peroxidase FeMC6*a with a pegylated aza-dibenzocyclooctyne (Figure 1A), to afford the "clickable" FeMC6*a-PEG_4@DBCO. This clickable biocatalyst may easily react with azide-functionalized molecules and/or nanomaterials to afford functional bioconjugates (Figure 1B).

Figure 1. Should be here

Herein we demonstrate that FeMC6*a-PEG_4@DBCO retains its catalytic and conformational behaviors when clicked with azide-functionalized moieties. Further, as a proof-of-principle, we selected azide-AuNPs as nanomaterials to assay the potential of the proposed clickable catalyst. On the basis of the results here presented, we foresee that FeMC6*a-PEG_4@DBCO could be clicked to a wide range of surface exposing the azide functionality, thus being useful for the preparation of functional bionanomaterials.

2. Experimental

2.1. Materials and instrumentations

All solvents, used in the synthesis and purification, as water, acetonitrile, trifluoroacetic acid (TFA), dimethylformamide (DMF), 2,2,2-trifluoroethanol (TFE), acetic acid, dimethylsulfoxide (DMSO) and ether, were anhydrous and HPLC grade, and were supplied by Romil (Cambridge, UK). Solvents with a higher degree of purity were used in the preparation of solutions for UV-Vis investigations (Ups grade). Trisodium citrate dihydrate as well as $HAuCl_4$ solution (30% w/w), ABTS (2,2'-azino-bis 3-ethylbenzothiazoline-6-sulphonic acid) and LA were purchased from Sigma Aldrich

(Taufkirchen, Germany). Phosphate salts (monobasic and dibasic) for buffers preparation, and H_2O_2 (30%, (*v*/*v*)) were provided by Fluka. UranyLess staining solution was purchased from Electron Microscopy Sciences. All buffer solutions were made by using water with a HPLC purity grade (Romil); *N*,*N*-diisopropylethylamine (DIEA) were obtained from Applied Biosystem. The activating agent 1-[bis(dimethylamino)methylene]-1H-1,2,3-triazole[4,5-b]pyridinium 3-oxid hexafluorophosphate (HATU) was from NovaBiochem, and the click reagent DBCO-PEG_4-NHS from Jena Bioscience. All reagents were used without further purification.

HPLC and LC-MS analysis were performed using a Shimadzu LC-10ADvp system equipped with an SPDM10Avp diode-array detector. ESI-MS spectra were recorded on a Shimadzu LC-MS-2010EV system with ESI interface and Shimadzu LC-MS solution Workstation software for data processing. Preliminary purifications and desalting are performed by flash chromatography (ISOLERA ISO-1SW Biotage with diode array detector). Purifications were accomplished by preparative RP-HPLC with Shimadzu LC-8A connected to a SPD-20A Shimadzu UV-Vis spectrophotometric detector. ESI-IT/TOF spectra were recorded on a Shimadzu LCMS-IT-TOF system with ESI interface and Shimadzu LC-MS solution Workstation software for the data. All analyses were performed with a Vydac C18 column (2.1 mm x 100 mm; 5µm), eluted with an H_2O 0.05 % TFA, (solvent A) and CH_3CN 0.05 % TFA (solvent B) linear gradient, from 10 to 95% (solvent B), over 37 minutes, at 0.2 mL min^{-1} flow rate. The optimized MS parameters were selected as followed: CDL (curved desolvation line) temperature 250°C; the block temperature 250 °C; the probe temperature 250 °C; detector gain 1.6kV; probe voltage +4.5kV; CDL voltage -15V. Nitrogen served as nebulizer gas (flow rate: 1.5 L min^{-1}).

The UV-Vis analysis and kinetic experiments were recorded with a Cary 60 spectrophotometer (Varian, Palo Alto, CA, USA), equipped with a thermostatic cell compartment, using quartz cuvettes with 0.10 cm, 0.01 cm and 1.00 cm path lengths. Wavelength scans were performed at 25°C from 200 to 800 nm, with a 600 nm min^{-1} scan speed. All data are blank corrected.

Circular Dichroism measurements were performed using a J-815 spectropolarimeter equipped with a thermostated cell holder (JASCO, Easton, MD, USA). CD spectra were collected using quartz cuvettes with 1.00 cm path length. at 25°C, from 260 to 200 nm with a 20 nm min^{-1} scan speed.

Nanoparticles and their derivatives were purified by centrifugation cycles through Sigma Refrigerated Centrifuge 2K15 with 12148-H or 12141-H rotors.

Iron and gold content of bioconjugate was quantified by ICP-MS analysis, using Aurora Bruker M90 instrumentation (Bremen, Germany). Aqua regia digestion procedure (90°C, 45 min) was adopted for organic component and gold degradation.

The linker conformation in FeMC6*a-PEG_4@LA was energy minimized using the conjugate gradient method, keeping the position of FeMC6*a enzyme fixed. The Discover package with the consistent valence force field (CVFF) [57-59] was employed.

All the molecular graphics pictures were generated with Visual Molecular Dynamics (VMD, http://www.ks.uiuc.edu/Research/vmd/) [60], and ChemDraw Ultra 12. Data analysis was made with Origin Pro 9.0 software (Origin Lab Corporation, Northampton, MA, USA), ImageJ software (National Institutes of Health, available free of charge at Web site rsb.info.nih.gov/ij/) and Kaleidagraph software (version 4.1.1, Synergy Software, Reading, PA, USA).

2.2 Synthesis of FeMC6*a-PEG_4@DBCO

Fe-MC6*a was previously synthesised and characterized, as described by Caserta *et al.* [30]. FeMC6*a-PEG_4@DBCO was obtained by coupling between FeMC6*a and the DBCO-PEG_4-NHS reagent (Figure 1A). The reaction was performed under stirring in anhydrous DMF as solvent, using 3 equivalents of DBCO-PEG_4-NHS ($2.77 \cdot 10^{-6}$ mol, 20µl of a stock solution 100 mg/ml in DMF) with respect to FeMC6*a ($9.25 \cdot 10^{-7}$ mol, 3.20 mg dissolved in 320 µl of DMF) in presence of DIEA (11 eq., 1.77 µl, pH ≈ 9). The reaction was left overnight at room temperature and was monitored by RP-HPLC (Shimazu SCL 10A VP) using a C18 column (GRACE Vydac 218TP C18, 5µ) eluted with H_2O/0.1% TFA (*v/v*) (solvent A) and acetonitrile/0.1% TFA (solvent B) in a linear gradient from 10

% to 50% of B in 30 min, with a flow rate of 1.0 mL·min^{-1}. The RP-HPLC chromatogram confirmed the formation of the desired product, on the basis of retention time shift (Figure 2).

Figure 2. Should be here

The excess of unreacted DBCO-PEG$_4$-NHS was removed by precipitation with methyl-*tert*-butyl ether (MTBE). The reaction mixture was slowly added to 1.5 mL of MTBE solution, which was kept at 0°C for 10 minutes. The mixture was then centrifuged at 8000 rpm, for 3 min. The supernatant was removed, and the precipitate was washed twice with MTBE, and dried.

2.3 Synthesis of 3-azidopropyl-5-(1,2-dithiolan-3-yl)pentanamide (LA@N_3)

The synthesis of the alkanethiol heterobifunctional linker used was performed in two steps: 1) synthesis of 3-azidopropan-1-amine; 2) coupling reaction between 3-azidopropan-1-amine and LA. 3-azidopropanamine was synthesized starting from 1,3-diazidopropane by hemireduction with triphenylphosphine (Staudinger reduction), following the protocol developed by Srinivasan *et al.* [61]. The reaction was carried out in biphasic media in order to obtain the desired product, avoiding

Scheme 1. Should be here

double reduction by product (1,3-diaminopropane) (Scheme 1A). The experimental procedure consisted into the addition of small portions of triphenylposphyine (PPh_3) to 1,3-diazidopropane in a biphasic mixture made of ethyl acetate (AcOEt)/diethyl ether (Et_2O) 1:1 (*v/v*) and 5 % (*v/v*) aqueous hydrochloric acid. In detail, 1,3-diazidopropane (1.5 mmol) was dissolved in Et_2O:AcOEt (1:1) (2 mL) and the aqueous phase (5 % HCl) (1.6 mL) was added under stirring. Then, small portions of triphenylphosphine (1 mmol) were added over 1 h. The reaction was kept for 1 h at 0°C and then left while stirring for 24 h at room temperature. The reaction was monitored *via* TLC using cyclohexane

as eluent. Afterwards, the reaction mixture was transferred to a separatory funnel, the organic layer was discarded, and the aqueous layer was extracted twice with methylene chloride (DCM) (2 mL). The resulting aqueous phase was carefully basified with 6 M NaOH and then extracted with DCM (3 x 2 mL). The organic fractions were pulled together and dried over Na_2SO_4. Finally, the excess of solvent was evaporated to dryness, to yield pure 3- azidopropanamine (quantitative yield).

Coupling between 3-azidopropanamine and LA was achieved by using HATU (1-[Bis(dimethylamino)methylene]-1H-1,2,3-triazole[4,5-b]pyridinium 3-oxid hexafluorophosphate) as activating agent (Scheme 1B). The coupling reaction was carried out by dissolving 4 mg of 3-azidopropanamine (1 eq) and 4.2 mg of LA (2 eq) in 1.5 mL of DMF. The solution was basified to pH ≈ 9 with DIEA and then 8.3 mg of HATU (1.1 eq) were added. Reaction mixture was left under stirring for 1 h and RP-HPLC-MS analysis was performed to identify the products. The mobile phase was made up of H_2O/0.1% TFA (solvent A) and CH_3CN/0.1% TFA (solvent B) linear gradient, from 20% to 95% (solvent B) over 30 min, at a 1 mL·min^{-1} flow rate. A Vydac C8 column (4.6x150 mm; 5 µm), was used in the LC-MS analysis. The mass spectrum displays a main peak at *m/z* 289.05 ($[M+H]^+$), in agreement with the theoretical mass (288.33 Da) of the desired compound *N*-(3-azidopropyl)-5-(1,2-dithiolan-3-yl)pentanamide (LA@N_3) . The reaction mixture was purified by preparative RP-HPLC on a C8 column (22 x 250 mm; 5 µm) with a linear gradient from 20 to 95% B over 50 minutes, at a 23 ml min^{-1} flow rate. The collected fractions were analyzed by LC, to confirm the purity of the product. The desired product exhibits absorption at λ = 333 nm, typical of disulfides containing compounds.

2.4 Synthesis of the FeMC6*a-PEG$_4$@LA

The click reaction between FeMC6*a-PEG$_4$@DBCO and LA@N_3 was performed in DMF solution using ≈ 2.5 eq of LA@N_3 (300 µl of a stock solution 4.6 mM in DMSO) respect to the clickable enzyme (Scheme 2).

Scheme 2. Should be here

The reaction was followed by RP-HPLC. The HPLC-MS analysis, after 4 hours, confirmed the formation of the desired product: experimental mass $[M+3H^+]/3$: 1438.6, $[M+4H^+]/4$: 1079.2 , $[M+5H^+]/5$: 863.6, consistent with the theoretical mass 4313.7 Da.

FeMC6*a-PEG_4@LA was purified by preparative RP-HPLC using a Vydac C18 column (250x10 mm). The mobile phase was made up of H_2O/0.1% TFA (solvent A) and CH_3CN/0.1% TFA (solvent B) and the product was eluted with a linear gradient from 5% to 80 % B over 55 minutes with a flow rate of 5 $mL \cdot min^{-1}$. RP-HPLC analysis of the collected fractions confirmed the purity of the product (data not shown), which was obtained with 69 % yield.

2.5 Synthesis of azide-AuNPs

Citrate-stabilized AuNPs were prepared *in situ* by the Turkevich method [62, 63]. An aqueous solution of $HAuCl_4$ (1 mM, 102 mL) was kept at reflux under stirring for 10 min. Once the gold solution was vigorously refluxing, an aqueous solution of pre-heated sodium citrate (39 mM, 10.2mL) was added quickly. The solution remained clear for about 10 s and then the color of the solution turned ruby-red, indicating the formation of gold nanoparticles. The suspension was allowed to heat for additional 30 min under vigorous stirring. The suspension was then allowed to cool to room temperature and stored in the dark at 4°C until further use.

The concentration of citrate-stabilized AuNPs in the stock solution was estimated directly from UV-Vis spectrum, by using the method reported by Fernig and coworkers [64]. As reported, the ratio between the absorbance at the SPRB ($A_{SPRB,}$) to the absorbance at 450 nm (A_{450}) can give an indication of the AuNPs diameter and therefore of its molar extinction coefficient. For an A_{SPRB}/A_{450} ratio of 1.65, the diameter of AuNPs was estimated to be ≅ 16 nm. From the value of A_{450} and using the calculated extinction coefficient ε_{450} of $2.67 \cdot 10^8\ M^{-1}\ cm^{-1}$, citrate-stabilized AuNPs concentration in the stock solution was estimated to be 6.15 nM.

The synthesis of azide-AuNPs was performed by ligand exchange reaction, using a slightly modified procedure of the protocol previously described by us [47]. In particular, 44 mL of citrate-stabilized AuNPs ([Au] ≅ 0.91 mM) were adjusted to pH ≅ 11 using a 1 M NaOH solution. Then a mixture of LA (3.05 mg, $1.48 \cdot 10^{-5}$ mmol) and LA@N_3 (0.47 mg, $1.64 \cdot 10^{-6}$ mmol) (LA:LA@N_3 ratio ≅ 9:1) dissolved in 6.4 mL of DMSO was added to the citrate-stabilized AuNPs. The suspension was incubated at room temperature in the dark, and the progress of the reaction was followed by UV-Vis analysis, evaluating the shift in the SPRB upon ligand exchange reaction. After 3h from ligands addition, the reaction mixture was centrifuged (7500 rpm, 40 min, 10°C) and the pellet was then resuspended in an equal volume of NaOH solution (pH = 11), yielding purified azide-AuNPs (AuNPs concentration ≅5.27 nM).

2.6 Synthesis of FeMC6*a-PEG$_4$@AuNPs

Conjugation of FeMC6*a-PEG$_4$@DBCO to AuNPs was obtained by the SPAAC reaction. The pH of the azide-AuNPs solution was adjusted to 11 with the dropwise addition of 1 M NaOH. To 6 mL of this stock solution (AuNPs concentration ≅5.27 nM), 191µg ($4.74 \cdot 10^{-8}$ mol) of FeMC6*a-PEG$_4$@DBCO, dissolved in anhydrous DMF, were added. The solution was incubated at room temperature in the dark, and the progress of the reaction was followed by UV-Vis analysis, evaluating the shift in the SPRB upon FeMC6*a conjugation.

After 3 hours, FeMC6*a-PEG$_4$@AuNPs were purified from the excess of catalyst, by cycles of centrifugation and resuspension (7500 rpm for 40 min at 10°C). After each centrifugation cycle, the supernatant was discarded, and the remaining pellet was re-dispersed in a NaOH solution (pH = 11). For the last centrifugation cycle, FeMC6*a-PEG$_4$@AuNPs were resuspended in NaOH solution (pH=11) with 50 %(*v*/*v*) of TFE, to remove excess FeMC6*a-PEG$_4$@DBCO non-covalently bound to the AuNPs surface [47]. Finally, the pellet was resuspended in NaOH solution (pH = 11) and promptly used for subsequent experiments.

2.7 AuNPs Physico-Chemical Characterization

Transmission electron microscopy (TEM) images were obtained in bright field mode using a TEM TECNAI G2 20ST operating at 120 kV. Copper grid with carbon film (Agar Scientific Ltd., product S160, 200 mesh) were used. The samples for TEM analysis were prepared by loading 5 µL drop for 60 seconds of citrate-stabilized AuNPs, azide-AuNPs, or FeMC6*a-PEG_4@AuNPs solutions onto carbon–coated copper grid using cold loading station. Protein shell of the FeMC6*a-PEG_4@AuNPs conjugates was visualized upon negative staining with UranyLess solution. The samples were washed using H_2O Ups (35µl drop, 3 times,10s) and stained using UranyLess solution (35µl drop, 3 times, 10s). Last wash was performed with H_2O (35µl drop, 10s) and letting grids to air–dry at room temperature overnight [65].

The histograms of the particle size distribution and the average particle diameter were calculated from the TEM images by using ImageJ software (National Institutes of Health, available free of charge at Web site rsb.info.nih.gov/ij/). At least 50 independent measurements were taken at different locations of the TEM images of the samples. The measurements were also confirmed by repeating the analysis on TEM images of independent samples.

ICP-MS analysis on the FeMC6*a-PEG_4@AuNPs conjugate allowed to determine the gold and iron content in the sample, that were respectively estimated to be 0.91 µM (Fe^{3+}) and 374 µM (Au^{3+}). Concentration of the enzyme-conjugated AuNPs solution was estimated as reported in the literature [66]. By assuming that all the gold is incorporated into spherical particles with the density of the bulk gold (ρ_{gold}= 19 g/cm^3) [67], AuNPs concentration can be obtained by dividing the concentration of atomic gold by the following equation:

$$\frac{4}{3}\pi r^3 \frac{\rho_{gold}}{AW_{gold}} \mathrm{A}$$

where r is the average radius of the particles from TEM data, A is Avogadro's number, and AW_{gold} is the atomic weight of gold (197.97 g/mol). By considering r = 7.1 nm, as derived from TEM analysis, the concentration of AuNPs in the sample was estimated to be 4.31 nM.

2.8 FeMC6*a Radius of Gyration Calculation

The radius of gyration (R_G) [68] for FeMC6*a molecule was calculated on the model structure as previously reported [47], by using the following equation:

$$R_G = \sqrt{\frac{1}{N}\sum_{i=1}^{N}(\vec{x}_i - \vec{x})^2}$$

where $\vec{x}_i$ is the position of the atom i in the model structure, x is the position of the centroid of the molecule, and N is the total number of non-hydrogen atoms. Calculation afforded a value of 9.03 Å (0.903 nm) for R_G value.

2.9 CD analysis

The samples for CD analysis were prepared by diluting an aliquot of FeMC6*a-PEG$_4$@AuNPs suspension with 10 mM phosphate buffer 50%(*v*/*v*) TFE, pH 6.5, to a final enzyme concentration of 0.3 μM. Mean residue ellipticities [θ] were calculated using the equation:

$$[\theta] = \frac{\theta_{obs}}{10 \cdot 1 \cdot C \cdot n}$$

in which θ_{obs} is the ellipticity measured in millidegrees, l is the path length of the cuvette in centimeters, C is the concentration in moles per liter, and n is the number of residues in the enzyme (24 residues).

2.10 Catalytic assays

All the catalytic data were acquired on a Varian Cary 60 spectrophotometer, at room temperature, under magnetic stirring, by using quartz cuvettes with 1.00 cm path lengths. Experiments were performed using the chromogenic substrate ABTS [69].The increase in absorbance of the $ABTS^{\bullet+}$ cation radical over time was followed at 660 nm ($\varepsilon_{660} = 1.44 \cdot 10^4$ M^{-1} cm^{-1}) for 10 minutes and used to extract the reaction initial rates (v_0). Substrate and hydrogen peroxide stock solutions were freshly prepared, and their initial concentrations were determined by UV-Vis spectroscopy (ABTS, ε_{340} = $3.66 \cdot 10^4$ M^{-1} cm^{-1}; H_2O_2, ε_{240}= 39.4 M^{-1} cm^{-1}). For each assay, a precise volume of oxidant (H_2O_2) was added to the FeMC6*a-PEG$_4$@AuNPs/ABTS mixture. The enzyme concentration was 27.3 nM

in each assay. Optimal experimental conditions were determined at 5 mM ABTS, 10 mM H_2O_2 by varying TFE percentage (0%, 30%, 50% (*v*/*v*)) in phosphate buffer 50 mM pH 6.5, or by varying pH: 4.5, 5.5 (acetate buffer), 6.5, 6, 7.5, 8.5 (phosphate buffer), 9.8 (carbonate buffer) at 50% (*v*/*v*) TFE. Kinetic parameters were determined by varying H_2O_2 concentration at fixed ABTS concentrations, and *viceversa*. All experiments were carried out in phosphate buffer (50 mM, pH 6.5), in the presence of TFE 50 %(*v*/*v*). H_2O_2 was varied in the 0–500 mM range (at 5 mM ABTS fixed concentration), while ABTS in the 0–10 mM range (at 100 mM H_2O_2 fixed concentration*)* The initial rates (v_0) of ABTS oxidation were plotted as function of the varying substrate concentration and fitted using a two-substrates Michaelis-Menten equation [70], reported below

$$v = \frac{[E]_0}{\frac{1}{k_{cat}} + \frac{K_{M_A}}{k_{cat}[A]} + \frac{K_{M_B}}{k_{cat}[B]}}$$

where *v* is the initial rate, $[E]_0$ is the enzyme concentration, [A] is the H_2O_2 concentration, [B] is the ABTS concentration. This allowed to extrapolate the catalytic constant (k_{cat}), and the Michaelis constants for both substrates (K_m^{ABTS} and $K_m^{H_2O_2}$).

For unconjugated FeMC6*a and clicked FeMC6*a-PEG_4@LA, catalytic assays were performed at 20 nM enzyme concentration, in the presence of 50 mM H_2O_2 and 2 mM ABTS, in phosphate buffer 50 mM pH 6.5 with TFE 50 %(v/v).

3. Results and discussion

3.1 Synthesis and reactivity of the "clickable" FeMC6*a: FeMC6*a-PEG_4@DBCO

The goal of this work was the development of a "clickable" artificial peroxidase, which can easily react with azide-functionalized surfaces, to afford functional nanomaterials. To this end, we settled on the use of the SPAAC reaction and modified FeMC6*a catalyst with an aza-dibenzocyclooctyne moiety (DBCO) (also referred to as DIBAC [53, 71]), linked to four polyethylene glycol (PEG) units. The presence of a linker based on four PEG units may ensure good solubility of the molecule in

aqueous solution upon DBCO insertion. Indeed, protein pegylation is widely applied to broaden the working conditions of biocatalysts, as pegylated enzymes often show improved solubility in various solvents, and increased stability in extreme condition of pH and temperatures [72]. Further, the PEG-linker flexibility should endow the enzyme with conformational mobility, upon loading on nanostructured surfaces. The presence of a single free amino group on the TD-Lys11 side chain allowed site-selective modification of the catalyst and afforded the PEGylated FeMC6*a, displaying the DBCO moiety (see Materials).

To investigate the reactivity of FeMC6*a-PEG_4@DBCO in SPAAC reaction, an azido-alkyl dithiolane reagent, i.e. LA@N_3 (see Scheme 2B), was used. Alkanethiols and alkanedithiolane ligands are frequently used for surface modification of inorganic nanoparticles [73], especially for AuNPs, as gold binds thiols with high affinity [74]. Thus, investigating the reactivity of FeMC6*a-PEG_4@DBCO with this reagent is crucial for successive work, aimed at immobilizing the artificial enzyme on different nanomaterials through click chemistry. The SPAAC reaction was carried out in DMF under stirring, using an excess (4 equivalents) of LA@N_3. The reaction proceeded to completion within one hour (data not shown). Purification of the reaction mixture by RP-HPLC and mass spectrometry analysis confirmed the formation of the desired product FeMC6*a-PEG_4@LA (yield 69%).

3.2 Use of the "clickable" FeMC6*a-PEG_4@DBCO for the development of functional nanomaterials

Recently, we have grown experience in functionalizing AuNP with MC artificial enzymes [47]; therefore, AuNPs capped with azide-terminated ligands were selected as a first nanomaterial, ready to react with the "clickable" FeMC6*a-PEG_4@DBCO. Azide-functionalized AuNPs have received enormous interest owing to their potential applications in click chemistry, and a variety of methods for their synthesis have been reported [73, 75, 76]. In this work, the ligand exchange strategy was selected to prepare monodisperse azide-functionalized AuNPs [73, 75, 76]. To this end, citrate-stabilized AuNPs were synthesized by the Turkevich method [63] and subsequently functionalized

with mixed-ligands, consisting of alkanethiols, bearing different chemical functionalities. To ensure stability of the colloidal solution, avoid nanoparticles aggregation, and reduce steric hindrance upon conjugation of the artificial catalyst on the AuNPs surface, composition of the ligand shell was strictly controlled [62]. Multifunctional coatings on AuNPs surface was obtained by using a mixture of LA and its azide-terminated derivative (LA@N_3), previously used for assaying the reactivity of FeMC6*a-PEG_4@DBCO. LA was selected as major component of the ligand shell (i.e. stabilizing ligand), ensuring AuNPs stability thanks to charge repulsion between the carboxylate groups (pKa 4.7 [77]) under basic pH conditions. To get the azide groups easily accessible for the click conjugation with the enzyme, the two alkanethiol ligands are made up by different alkyl chain lengths, with the longer chain bearing the azide (LA@N_3). Finally, to reduce azido-groups crowding on the AuNPs surface, thus increasing the click-reaction efficiency [76, 78], a 9:1 molar ratio of stabilizing ligand (LA) to azide-terminated ligand (LA@N_3) was used. Following a previously developed protocol [47], the ligand exchange reaction was carried out by addition of the LA/LA@N_3 mixture in DMSO, to citrate-stabilized AuNPs in water (pH 11), under stirring in dark (0.4094 equivalents of ligands with respect to Au). Upon addition of the alkanethiol mixture, a shift in the SPRB of the citrate-stabilized AuNPs, from 520 nm to 523 nm, was observed (data not shown). This finding is consistent with changes in refractive index on nanoparticles surface, caused by the occurred ligand exchange reaction [79]. The AuNPs solution was then purified, through several cycles of centrifugation and resuspension. After each cycle, the supernatants were discarded and the pellet dispersed in equal volume of NaOH (pH=11) and centrifuged again. The mixed azide- and carboxyl-terminated AuNPs were stable under these experimental conditions, as the absorption spectra showed no broadening of SPRB neither shift in the absorption maximum.

Conjugation of the "clickable" FeMC6*a-PEG_4@DBCO, *via* SPAAC reaction, with the azide-AuNPs was performed by adding a solution of the enzyme (47.4 nmol of FeMC6*a-PEG_4@DBCO in anhydrous DMF, excess 1500 equivalents) to the AuNPs aqueous solution (6.0 mL, 5.27 nM, pH 11), under vigorous stirring. The reaction was left under stirring overnight. Unbound FeMC6*a-

PEG_4@DBCO was removed from the FeMC6*a-PEG_4@AuNPs conjugate through several cycles of centrifugation. After each cycle, the supernatants containing the unbound enzyme were discarded and the pellet containing the conjugate was resuspended in an equal volume of NaOH (pH=11), in order to preserve stability of the colloidal solution. As final step in the conjugation procedure, the FeMC6*a-PEG_4@AuNPs were washed with a 1:1 solution of NaOH (pH=11): TFE (*v/v*). This washing procedure was performed in order to inhibit adsorption and/or non-covalent aggregation of FeMC6*a-PEG_4@DBCO onto the AuNPs surface, thanks to the high solvation properties of TFE and enzyme solubility [47].

3.3 Characterization of the FeMC6*a-based nanomaterial.

3.3.1 UV-visible characterization of FeMC6*a-PEG4@AuNPs

Conjugation of FeMC6*a to AuNPs by SPAAC reaction was ascertained by UV-Visible spectroscopy. Figure 3 reports the superposition of the visible spectra of azide-AuNPs (red line) and of the FeMC6*a-PEG_4@AuNPs conjugate (black line).

Compared to azide-AuNPs (λ_{max}=523 nm), the conjugate shows a maximum absorption of SPRB at 528 nm. The slight SPRB shift (5 nm) observed upon click reaction between azide-AuNPs and FeMC6*a-PEG_4@AuNPs is indicative of a change in the refractive index of the nanoparticle surface, likely caused by the presence of the covalently bound catalyst [79]. The absence of significant SPRB broadening suggests that, upon FeMC6*a-PEG_4 coating, AuNPs remained well dispersed without any aggregation in the colloidal suspension. The absorption band around 387 nm in the conjugate spectrum can be attributed to the Soret absorption band of Fe(III)MC6*a [30], thus providing a direct evidence of the successful catalyst conjugation to AuNPs.

Figure 3. Should be here

3.3.2 TEM analysis of the FeMC6*a-PEG4@AuNPs conjugate

The morphology and size distribution of AuNPs upon conjugation with the clickable artificial enzyme were assessed by Transmission Electron Microscopy (TEM) analysis. Figure 4 reports a comparison of the TEM images of the azide-AuNPs (Figure 4A-C) and FeMC6*a-PEG_4-AuNPs (Figure 4D-F). AuNPs appeared uniform in size and shape. The mean particle size and standard deviation were determined from nanoparticles statistic measurements using ImageJ software on TEM analysis on the azide-AuNPs (Figure 4C), giving an average core diameter of 14.2±1.4 nm. Some clustering, visible in the TEM images, was likely due to the deposition and drying process on the carbon-coated grids [80], as UV-Vis spectrum of the azide-AuNPs was indicative of no aggregate formation (Figure 3). TEM images of FeMC6*a-PEG_4@AuNPs, analyzed upon negative staining with the UranyLess reagent, allowed for highlighting of the protein shell as a white halo around each AuNPs (Figure 4E). An average diameter of 20.7 ± 0.1 nm was measured for the FeMC6*a-PEG_4@AuNPs conjugate (Figure 4F), with a protein shell thickness of 3.3± 0.3 nm. The observed deviation for the protein layer thickness confirms that the adopted coating technique generates highly homogenous surfaces.

Figure 4. Should be here

Inductively coupled plasma mass spectrometry (ICP-MS) was used to quantify the amount of FeMC6*a loaded on each AuNPs. The concentration of FeMC6*a in the AuNPs solution was determined by quantifying the heme moiety on the basis of the total iron content of the sample (0.91 µM). Given an AuNPs concentration of 4.31 nM (see Materials and Methods), an average loading of ≅ 210 FeMC6*a molecules *per* nanoparticle was obtained.

The maximum theoretical number of enzyme molecules (N_{max}) that can be loaded on each spherical AuNP was calculated with the model described by Mattoussi et al [81], using the following equation:

$$N_{max} = 0.65 \times \frac{(R_{complex}^3 - R_{AuNP}^3)}{R_{protein}^3}$$

where $R_{complex}$ is the AuNP-protein complex radius, R_{AuNP} is the gold nanoparticle radius, and $R_{protein}$ is the radius of the protein. The model, through geometrical considerations, assumes that the proteins are close-packed around each AuNPs as spheres, and adjusts the volume ratio by the filling factor for hard sphere, calculated to be 0.65 [82]. Specifically, R_{AuNP} comprises the sum of the gold core nanoparticles radius (R_{Gold}) and the length of the spacer arm connecting FeMC6*a to the AuNP surface (R_{spacer}) (Figure 5A).

Figure 5. Should be here

This spacer, comprising LA, the PEG-containing linker and the side chain of Lys residue, is highly flexible. Thus, an average estimation of its length can be obtained by evaluating the possible conformations this spacer may adopt in water. To this end, we roughly considered the entire spacer as a polymer chain composed by *n* repeating ethylene glycol units. The thickness of this spacer on the AuNPs surface can be related to the polymer conformation, that can be described by the Flory radius (R_F) [83], according to the following equation:

$$R_F = \alpha \cdot n^{\nu}$$

where *n* is the number of monomers *per* polymer chain and α is the length of one monomer in nanometers. For polymer chain in solution, as the monomers display finite volume, excluded volume interaction should also be considered. Flory equation thus includes a scaling exponent *v*, which accounts for monomer interactions and calculated to be 0.6 [84]. For a monomer unit in *trans-trans-trans* (*ttt)* conformation, α value is 0.35 nm. The α value is 0.28 nm when a *trans-trans-gauche (ttg)* conformation is adopted [85]. Considering that PEG retains a *ttg* structure in water [85], the Flory radius for the PEG-containing linker ($n = 6$), was calculated to be $R_F = 0.28 \times 6^{0.6} = 0.82$ nm. Given that alkyl chains covering gold surface are generally assembled in ordered monolayers [86] and lysine residue may be considered as the junction unit, the LA and Lys side chains were prudently

approximated to an all-*trans* extended polymer chain consisting of a total of 5 monomer units. This calculation gave an estimate length of R_F=0.35×$5^{0.6}$=0.92 nm for this part of the spacer.

On the basis of this estimation, R_{AuNP} was calculated to be ≅ 8.84 nm, by the sum of the gold core radius (R_{gold}= 7.1 nm as determined from TEM data) and the length of the entire spacer (R_{spacer}=1.74 nm from the above calculation). $R_{complex}$ comprises the sum of R_{AuNP} and the diameter of FeMC6*a protein (see Figure 5A). As previously described by us, MCs are characterized by a cylindrical shape [47]. Thus, to consider all possible randomly oriented cylinder molecules with respect to the AuNP, the radius of gyration (R_G) was calculated (see Experimental), and the value of 2xR_G (1.8 nm) was used as FeMC6*a diameter for the calculation of $R_{complex}$.

Using the above data, the maximum theoretical number of FeMC6*a molecules per AuNP was estimated to be N_{max}≅ 458. Comparison of the experimentally determined actual loading by ICP mass analysis (≅210, see above) with the theoretical N_{max} suggests the formation of an enzyme monolayer around each AuNPs [47]. This finding is further supported by the protein shell thickness measured by TEM, as the sum of the calculated FeMC6*a diameter and spacer length (3.54 nm) is in good agreement with the experimental value.

Moreover, to further support our results, we used molecular modeling to gain some insights about the relative arrangement of FeMC6*a and the spacer arm. To this end, we modeled the linker structure of FeMC6*a-PEG_4@LA by energy minimization in *vacuo* (Figure 5B). Starting from an all-*trans* conformation, upon structure minimization, the extended linker folds back, providing a hydrophobic interaction between DBCO and the PEG moiety, and a hydrogen bond between the Lys and LA. With this arrangement the distance between the sulfur atom of the LA and the Cα atom of the Lys residue is 1.5 nm, thus being in good agreement with the previous calculation using Flory radius description.

3.3.3 Conformational properties of FeMC6*a upon immobilization on AuNPs

CD spectroscopy was used to check whether the conjugation on AuNPs affected the conformational properties of the artificial enzyme. Figure 6 reports the CD spectrum of FeMC6*a-PEG_4@AuNPs

conjugate (black line). The spectrum displays two minima at 222 and 208 nm, respectively, which indicate that the peptide chains fold into a α-helix secondary structure. Even though the magnitude of [θ_{222}] (θ_{222}=-11830 deg cm^2 dmol^{-1} res^{-1}) is slightly lower than that observed for the freely diffusing enzyme (θ_{222} =-15500 deg cm^2 dmol^{-1} res^{-1}, Figure 6 red line) [30], the overall helical conformation of the artificial catalyst is retained upon clicking on AuNPs. This represents an outstanding result, which demonstrates that the structural robustness of the scaffold allows FeMC6*a being immobilized onto surfaces without losing its conformational properties.

Figure 6. Should be here

3.4 Catalytic activity of the FeMC6*a-PEG$_4$@AuNPs nanomaterial.

To analyze whether FeMC6*a retains its catalytic behaviors once immobilized on surface, the peroxidase activity of FeMC6*a-PEG$_4$@AuNPs was screened, using ABTS as substrate and H_2O_2 as oxidizing agent, under the optimal experimental conditions (50 mM phosphate buffer pH 6.5, 50% TFE *v/v*) previously determined for FeMC6*a. A catalytic control assay was first performed on both the supernatant and the resuspended pellet of the last washing/centrifugation step of the synthetic procedure. Activity was detected in the nanoparticles resuspended pellet, whereas only background autoxidation was detected in the supernatant. This result excludes the presence of unconjugated free enzyme molecules in the AuNP-conjugate solution, and it is the first evidence that FeMC6*a retains peroxidase activity when conjugated to the AuNPs.

Once ascertained that FeMC6*a is still active when immobilized, the effect of TFE content and pH on the catalytic activity of FeMC6*a-PEG$_4$@AuNP was investigated, as such parameters were demonstrated to strongly influence FeMC6*a peroxidase activity [30]. The initial rate of ABTS oxidation (v_0) as a function of TFE concentration was assayed in phosphate buffer 50 mM (pH=6.5). As observed for the freely diffusing unmodified catalyst [30], the v_0 increases upon TFE addition up to 50% TFE (*v/v*). Moreover, the v_0 pH profile showed a bell-shaped curve, with a maximum at pH

6.5 (data not shown).

The kinetic parameters of FeMC6*a-PEG$_4$@AuNPs conjugate were determined by varying H_2O_2 concentration using fixed concentrations of ABTS, and *vice versa*, in 50 mM phosphate buffer pH 6.5, 50% TFE (*v/v*). The initial rates of ABTS oxidation (v_0) were plotted as a function of both substrate concentrations (Figure 7). Interestingly, the enzyme activity followed a typical Michaelis–Menten kinetics, as observed for the freely diffusing enzyme.

Figure 7. Should be here

Table 1 reports the k_{cat} (turnover frequency) and K_m (Michaelis–Menten constant) values for FeMC6*a and FeMC6*a-PEG$_4$@AuNPs. Analysis of the data revealed a marked decrease of the k_{cat} value when moving from the freely diffusing enzyme (k_{cat} 5800 s^{-1}) to the FeMC6*a-PEG$_4$@AuNPs bioconjugate (k_{cat} 110 s^{-1}), and a slight increase in the K_m value for ABTS. This result, although unfavorable, is not surprising. In fact, the catalytic efficiency of natural enzymes can broadly change upon immobilization onto different surfaces and/or AuNPs [87-89]. Upon immobilization on nanoparticles, enzymes activity may be reduced due to partial loss of the catalyst active structure. In the case of FeMC6*a-PEG$_4$@AuNPs, this may be excluded as the CD spectrum suggests the helical structure being preserved upon conjugation. To ascertain whether the observed reduction of the enzyme activity upon immobilization might be ascribed to the chemical modification of the enzyme by pegylation and clicking, the catalytic behaviors of FeMC6*a-PEG$_4$@LA were assayed and compared to those of the unmodified FeMC6*a. At 20 nM enzyme concentration (2 mM ABTS, 50 mM H_2O_2 in 50 mM phosphate buffer pH 6.5 50% TFE (*v/v*)), the initial rate (v_0) for ABTS conversion were determined to be 0.017 mM s^{-1} and 0.014 mM s^{-1} for FeMC6*a-PEG$_4$@LA and FeMC6*a, respectively. This finding suggests that pegylation and SPAAC reaction does not influence FeMC6*a reactivity. Thus, other factors may account for the reduced activity observed upon enzyme immobilization on AuNPs, as for example the limited diffusion of the substrates to the active site.

Indeed, the presence of the negatively charged carboxylate groups on the AuNPs surface may influence binding of the ABTS substrate to the active site, thus increasing K_m value.

A deep study on the factors affecting the catalytic parameters of the FeMC6*a enzyme when clicked on AuNPs is underway, as in this work immobilization on nanoparticles was selected as a proof-of-principle study for the application of FeMC6*a-PEG_4@DBCO as a clickable artificial peroxidase, useful for the development of functional nanomaterials.

4. Conclusions

In this work, we demonstrated the feasibility of the mimochrome derivative FeMC6*a to act as "clickable" artificial peroxidases. The functionalization of FeMC6*a with an alkyne group, afforded FeMC6*a-PEG_4@DBCO, a catalyst to be applied in SPAAC reaction with azido-containing entities, either small molecules or nanomaterials. Indeed, FeMC6*a-PEG_4@DBCO rapidly reacted with LA@N_3 to give the "clicked" derivative FeMC6*a-PEG_4@LA. This molecule retained the catalytic activity of the unmodified FeMC6*a catalyst, thus demonstrating that chemical modification of the molecule by pegylation and SPPAC reaction does not influence the reactivity of the active site. Moreover, AuNPs were used as a simple nanomaterial to exploit the feasibility of the clickable FeMC6*a-PEG_4@DBCO in being confined to a nanosurface. The conjugates FeMC6*a-PEG_4@AuNPs were found to be catalytically active toward peroxidase reaction, even though a decrease in the catalyst efficiency was observed upon conjugation. It is well ascertained that is very difficult to find the optimal methods to immobilize an enzyme without losing its activity, and usually iterative improvements through trial and error are needed. The results herein reported represent a proof of concept for the application of mimochromes in the development of a wide range of functional nanomaterials, as FeMC6*a-PEG_4@DBCO can be prone to react with any kind of azide-terminated surface.

5. Acknowledgements

The authors wish to thank Dr. Monica Grasso and Roberta Biondi for technical assistance.

6. Funding

This work was supported by Campania Region "Programma Operativo FESR Campania 2014–2020, Asse 1", [CUP B63D18000350007].

7. References

[1] Nastri, F., D'Alonzo, D., Leone, L., Zambrano, G., Pavone, V., Lombardi, A. (2019) *Trends Biochem. Sci.*, **44**, 1022-1040.

[2] Yu, F., Cangelosi, V. M., Zastrow, M. L., Tegoni, M., Plegaria, J. S., Tebo, A. G., Mocny, C. S., Ruckthong, L., Qayyum, H., Pecoraro, V. L. (2014) *Chem. Rev.*, **114**, 3495-3578.

[3] Lin, Y.-W. (2017) *Coord. Chem. Rev.*, **336**, 1-27.

[4] Petrik, I. D., Liu, J., Lu, Y. (2014). *Curr. Opin. Chem. Biol.*, **19**, 67-75

[5] Schwizer, F., Okamoto, Y., Heinisch, T., Gu, Y., Pellizzoni, M. M., Lebrun, V., Reuter, R., Köhler, V., Lewis, J. C., Ward, T. R. (2018) *Chem. Rev.*, **118**, 142-231.

[6] Hyster, T. K., Ward, T. R. (2016) *Angew. Chem. Int. Ed.*, **55**, 7344-7357.

[7] Grayson, K. J., Anderson, J. R. (2018) *Curr. Opin. Struct. Biol.*, **51**, 149-155.

[8] Mahy, J.-P., Marechal, J.-D., Ricoux, R. (2015) *Chem. Commun*., **51**, 2476-2494.

[9] Lombardi, A., Pirro, F., Maglio, O.,Chino, M., DeGrado, W. F. (2019) *Acc. Chem. Res.*, **52**, 1148-1159.

[10] Nastri, F. ,Chino, M., Maglio, O., Bhagi-Damodaran, A., Lu, Y., Lombardi, A. (2016) *Chem. Soc. Rev.*, **45**, 5020-5054.

[11] Chino, M., Leone, L., Zambrano, G., Pirro, F., D'Alonzo, D., Firpo, V., Aref, D., Lista, L., Maglio, O., Nastri, F., Lombardi, A. (2018) *Biopolymers*, **109**, e23107.

[12] Chino, M., Maglio, O., Nastri, F., Pavone, V., DeGrado, W. F., Lombardi, A. (2015) *Eur. J. Inorg. Chem.*, **2015**, 3371-3390.

[13] Oohora, K., Onoda, A., Hayashi, T. (2019) *Acc. Chem. Res.*, **52**, 945-954.

[14] Mocny, C. S., Pecoraro, V. L. (2015) *Acc. Chem. Res.*, **48**, 2388-2396.

[15] Zastrow, M. L., Pecoraro, V. L. (2013) *Coord. Chem. Rev.*, **257**, 2565-2588.

[16] Churchfield, L. A., Tezcan, F. A. (2019) *Acc. Chem. Res.*, **52**, 345-355.

[17] Le, J. M., Bren, K. L., (2019) *ACS Energy Lett.*, **4**, 2168-2180.

[18] Alcala-Torano, R., Sommer, D.J., Bahrami Dizicheh, Z., Ghirlanda, G. (2016) *Methods Enzymol*, **580**, 389-416.

[19] Lewis, J. C. (2019) *Acc. Chem. Res.*, **52**, 576-584.

[20] Natoli, S. N., Hartwig, J. F. (2019) *Acc. Chem. Res.*, **52**, 326-335.

[21] Roelfes, G. (2019) *Acc. Chem. Res.*, **52** ,545-556.

[22] Arnold, F.H. (2018) *Angew. Chem. Int. Ed.* **57**, 4143-4148.

[23] Renata, H., Wang, Z.J., Arnold, F.H. (2015) *Angew. Chem. Int. Ed.* **54**, 3351-3367.

[24] Lombardi, A., Nastri, F., Pavone, V. (2001) *Chem. Rev.*, **101**, 3165-3190.

[25] Lombardi, A., Nastri, F., Marasco, D., Maglio, O., Sanctis, G. D., Sinibaldi, F., Santucci, R., Coletta, M., Pavone, V. (2003) *Chem. Eur. J.*, **9**, 5643-5654.

[26] Di Costanzo, L., Geremia, S., Randaccio, L., Nastri, F., Maglio, O., Lombardi, A., Pavone, V. (2004) *J. Biol. Inorg. Chem.*, **9**, 1017-1027.

[27] Nastri, F., Lista, L., Ringhieri, P., Vitale, R., Faiella, M., Andreozzi, C., Travascio, P., Maglio, O., Lombardi, A., Pavone, V. (2011) *Chem. Eur. J.*, **17**, 4444-4453.

[28] Vicari, C., Saraiva, I.H., Maglio, O., Nastri, F., Pavone, V., Louro, R.O., Lombardi, A. (2014) *Chem. Commun.*, **50**, 3852-3855.

[29] Vitale, R., Lista, L., Cerrone, C., Caserta, G., Chino, M., Maglio, O., Nastri, F., Pavone, V., Lombardi, A. (2015) *Org. Biomol. Chem.*, **13**, 4859-4868.

[30] Caserta, G., Chino, M., Firpo, V., Zambrano, G., Leone, L., D'Alonzo, D., Nastri, F., Maglio, O., Pavone, V., Lombardi, A. (2018) *ChemBioChem*, **19**, 1823-1826.

[31] Leone, L., D'Alonzo, D., Balland, V., Zambrano, G., Chino, M., Nastri, F., Maglio, O., Pavone, V., Lombardi, A. (2018) *Front. Chem.*, **6**, 590.

[32] Firpo, V., Le, J. M., Pavone, V., Lombardi, A., Bren, K. L. (2018) *Chem. Sci.*, **9**, 8582–8589.

[33] Le, J.M., Alachouzos, G., Chino, M., Frontier, A. J., Lombardi, A., Bren, K.L (2020) *Biochemistry*, **59**, 1289-1297.

[34] Oliva, R., Chino, M., Pane, K., Pistorio, V., De Santis, A., Pizzo, E., D'Errico, G., Pavone, V., Lombardi, A., Del Vecchio, P., Notomista, E., Nastri, F., Petraccone, L. (2018) *Sci. Rep*., **8**, 8888.

[35] Hanefeld, U., Gardossib, L., Magnerc, E. (2009) *Chem. Soc. Rev.*, **38**, 453-468.

[36] Sheldon, R. A., van Pelt, S. (2013) *Chem. Soc. Rev.*, **42**, 6223-6235.

[37] Ansari, S. A., Husain, Q. (2012) *Biotechnol. Adv.*, **30**, 512-523.

[38] Mohamad, N.R., Marzuki, N.H.C., Buang, N.A., Huyop, F., Wahab, R.A. (2015) *Biotechnol. Biotechnol. Equip.*, **29**, 205-220.

[39] Zucca, P., Fernandez-Lafuente, R. , Sanjust, E. (2016) *Molecules*, **21**, 1577.

[40] Bilal, M., Iqbalb, H. M. N., Guoa, S., Hua, H., Wanga, W., Zhang, X. (2018) *Int. J. Biol. Macromol,* **108**, 893-901.

[41] Zdarta, J., Meyer, A. S., Jesionowski, T., Pinelo, M. (2018) *Catalysts*, **8**, 92-119.

[42] Chen, M., Zeng, G., Xu, P., Lai, C., Tang, L. (2017) *Trends Biochem. Sci.*, **42**, 914-930.

[43] Cipolatti, E. P., Silva, M. J. A., Klein, M., Feddern, V., Feltes, M. C., Oliveira, J. V., Ninow, J. L., de Oliveira, D. (2014) *J. Mol. Cat. B*, **99**, 56-67.

[44] Auriemma, F., De Rosa, C., Malafronte, A., Di Girolamo, R., Santillo, C., Gerelli, Y., Fragneto, G., Barker, R., Pavone, V., Maglio, O., Lombardi A. (2017) *ACS Appl. Mater. Interfaces*, **9**, 29318-29327.

[45] Ranieri, A., Monari, S., Sola, M., Borsari, M., Battistuzzi, G., Ringhieri, P., Nastri, F., Pavone, V., Lombardi, A. (2010) *Langmuir*, **26**, 17831-17835.

[46] Vitale, R., Lista, L., Lau-Truong, S., Tucker, R.T., Brett, M.J., Limoges, B., Pavone, V., Lombardi, A., Balland, V.. (2014) *Chem. Commun.*, **50**, 1894–1896.

[47] Zambrano, G., Ruggiero, E., Malafronte, A., Chino, M., Maglio, O., Pavone, V., Nastri, F., Lombardi, A. (2018) *Int. J. Mol. Sci.*, 19, 2896.

[48] Kolb, H. C., Finn, M. G., Sharpless, K. B. (2001) *Angew. Chem. Int. Ed.*, **40**, 2004-2021.

[49] Sletten, E.M., Bertozzi, C. R. (2009) *Angew. Chem. Int. Ed Engl.*, **48**, 974-6998.

[50] Liang, L., Astruc, D. (2011) *Coord. Chem. Rev*. **255**, 2933-2945.

[51] Jewett, J.C., Bertozzi, C. R. (2010) *Chem. Soc. Rev.*, **39**, 1272-1279.

[52] Agard, N. J., Prescher, J. A., Bertozzi, C. R. (2004) *J. Am. Chem. Soc*., **126**, 15046-15047.

[53] Dommerholt, J., Rutjes, F. P. J. T., van Delft, F. L. (2016) *Top Curr. Chem. (Z)* **374**, 16.

[54] Debets, M.F., Van Berkel, S. S., Dommerholt, J., Dirks, A. T. J., Rutjes, F.P.J.T., Van Delft, F. L. (2011) *Acc. Chem. Res.*, **44**, 805-815.

[55] Chino, M., Leone, L., Maglio, O., D'Alonzo, D., Pirro, F., Pavone, V., Nastri, F., Lombardi, A. (2017) *Angew. Chem. Int. Ed. Engl*. **56**, 15580-15583.

[56] Chino, M., Leone, L., Maglio, O., Lombardi, A. (2016) *Methods Enzymol*, **580**, 471-499.

[57] Lifson, S., Hagler, A. T., Dauber, P. J. (1979) *J. Am. Chem. Soc.*, **101**, 5111-5121.

[58] Hagler, A. T., Lifson, S., Dauber, P. J. (1979) *J. Am. Chem. Soc.*, **101**, 5122-5130.

[59] Hagler, A. T., Dauber, P. J., Lifson, S. (1979) *J. Am. Chem. Soc.*, **101**, 5131-5140.

[60] Humphrey, W., Dalke, A. and Schulten, K. (1996) *J. Mol. Graph.* **14,** 33-38.

[61] Srinivasan, *R.,* Tan, *L. P.,* Wu, H., Yang, P.-Y., Kalesh, K. A., Yao, S. Q. (2009) *Org. Biomol. Chem.*, **7**, 1821-1828.

[62] Zhao, P., Li, N., Astruc, D. (2013). *Coord. Chem. Rev.*, **257**, 638-665.

[63] Turkevich, J., Stevenson, P.C., Hillier, J. (1951) *Discuss. Faraday Soc*., **11**, 55-75.

[64] Haiss, W., Thanh, N.T.K., Aveyard, J., Fernig, D.G. (2007) *Anal. Chem*., **79**, 4215-4221.

[65] Rames, M., Yu, Y., Ren, G. (2014) *J. Vis. Exp.* **90**, e51087.

[66] Jamison, J.A., Bryant, E.L., Kadali, S.B.,Wong, M.S., Colvin, V.L., Matthews, K.S., Calabretta, M.K. (2011) *J. Nanopart. Res*., **13**, 625-636.

[67] Frens, G. (1973) *Nat. Phys. Sci*., **241**, 20-22.

[68] Lobanov, M.Y., Bogatyreva, N.S., Galzitskaya, O.V. (2008) *Mol. Biol.*, **42**, 623-628.

[69] Childs, R.E., Bardsley,W.G. (1975) *Biochem. J.*, **145**, 93-103.

[70] Johnson ,K. A. (2013) *FEBS Letters,* **587** 2753-2766.

[71] Debets, M.F., Van Berkel, S. S., Schoffelen, S., Rutjes, F.P.J.T., van Hest, J.C.M., Van Delft, F. L. (2010) *Chem. Commun.*, **46**, 97-99.

[72] Hsieh, Y.-P., Lin, S.-C. (2015) *Process Biochemistry,* **50** 1372-1378.

[73] Li, N., Binderri, W. H. (2011) *J. Mater. Chem*., **21**, 16717-16734.

[74] Lin, Y.-C., Yu, , B.-Y., Lin, W.-C., Lee ,S.-H., Kuo, C.-H., Shyue, J.-J. (2009) *J. Colloid Interface Sci.* **340**, 126-130.

[75] .Zhang, M.-X., Huang, B.-H., Sun, X.-Y., Pang, D.-W. (2010) *Langmuir*, **26**, 10171-10176.

[76] Elliott, E. W., Ginzburg, A. L., Kennedy, Z. C., Feng, Z., Hutchison ,J. E. (2017) *Langmuir*, **33**, 5796-5802.

[77] Krishnan, C. V., Garnett, M. (2011) *Int. J. Electrochem. Sci.*, **6**, 3607-3630.

[78] Thode, C.J.,Williams, M.E. (2008) *J. Colloid Interface Sci.* **320**, 346-352.

[79] Templeton, A.C., Pietron, J.J., Murray, R.W., Mulvaney, P. (2000) *J. Phys. Chem. B*, **104**, 564-570.

[80] Michen, B., Geers, C., Vanhecke, D., Endes, C., Rothen-Rutishauser, B., Balog, S., Petri-Fink, A. (2015) *Sci. Rep*., **5**, 9793.

[81] Mattoussi, H., Mauro, J.M., Goldman, E.R., Anderson, G.P., Sundar, V.C., Mikulec, F.V., Bawendi, M.G. (2000) *J. Am. Chem. Soc*., **122**, 12142-12150.

[82] Cebula, J., Ottewill, R.H., Ralston, J., Pusey, P.N. (1981) *J. Chem. Soc. Faraday Trans. 1*, **77**, 2585-2612.

[83] Flory, P.J.(1967) Principles of Polymer Chemistry, Cornell University, Ithaca.

[84] Ma, Z., LeBard, D.N., Loverde, S.M., Sharp, K.A., Klein, M.L., Discher, D.E., Finkel, T. H. (2014) *PLOS ONE*. **9**, e112292.

[85] Oesterhelt, F., Rief, M., Gaub, H.E. (1999*) New J. Phys. 1* 6.1-6.11.

[86] Ulman, A. (1996) *Chem. Rev*., **96**, 1533-1554.

[87] Jia, H., Zhu, G., Wang, P. (2003) *Biotechnol. Bioeng*., **84**, 406-414.

[88] Rodrigues, R.C., Ortiz, C., Berenguer-Murcia, A., Torres, R., Fernández-Lafuente, R. (2013) *Chem. Soc. Rev*., **42**, 6290-6307.

[89] Santos, J.C.S.D., Barbosa, O., Ortiz, C., Berenguer-Murcia, A., Rodrigues, R.C., Fernandez-Lafuente, R. (2015) *ChemCatChem*., **7**, 2413-2432.

Table 1. Catalytic parameters for FeMC6*a and FeMC6*a-PEG_4@AuNPS

Enzyme	K_m^{ABTS} (mM)	$K_m^{H_2O_2}$ (10^2 mM)	k_{cat} (10^2 s^{-1})	k_{cat}/K_m^{ABTS} (10^3 mM^{-1} s^{-1})	$k_{cat}/K_m^{H_2O_2}$ (mM^{-1} s^{-1})
FeMC6*a	0.09±1	4.4±0.5	58±3	64±8	13±2
FeMC6*a@AuNPs	0.193± 0.005	2.16±0.04	1.10±0.03	0.570± 0.001	0.509±0.003

Figure legends.

Figure 1. Clickable artificial peroxidase. A) Functionalization of FeMC6*a with the pegylated aza-dibenzocyclooctyne. B) Immobilization of FeMC6*a-PEG_4@DBCO on AuNPS, *via* SPAAC, to afford catalytically active nanomaterial.

Figure 2. Comparison of the RP-HPLC chromatogram of FeMC6*a (red line) and of FeMC6*a-PEG_4@DBCO (black line).

Figure 3. UV-Vis spectra of surface modified AuNPs: azide-AuNPs (red line, nanoparticle concentration 5.27 nM) and FeMC6*a-PEG_4@AuNPs (black line, nanoparticle concentration 4.31 nM).

Figure 4. TEM images of the synthesized AuNPs, along with the corresponding size distribution histograms. A-C) Azide-AuNPs. D-F) FeMC6*a-PEG_4@AuNPs conjugate. The samples were stained with UranyLess before observation.

Figure 5. A) Schematic representation of the packing of FeMC6*a around a single AuNP. The dimensions of each conjugate component used for calculating N_{max} (the maximum theoretical number of enzyme molecules that can be loaded on each spherical AuNP) are shown. B) FeMC6*a-PEG_4@LA molecular model. Backbone is represented as ribbon. *(D)* and *(TD)* chains are depicted in gold and in green, respectively. The distance between the sulfur atom of LA and the Cα atom of the Lys residue is also indicated. The model structure was generated with VMD [60].

Figure 6. Superposition of the CD spectra of FeMC6*a-PEG_4@AuNPs and FeMC6*a (10 mM phosphate buffer (pH 6.5) 50% TFE (*v/v*).

Figure 7. Peroxidase activity of FeMC6*a-PEG_4@AuNPs: A) initial rate dependence towards ABTS concentration; B) initial rate dependence towards H_2O_2 concentration. Reaction conditions were: 50.0 mM phosphate buffer pH 6.5 50% TFE (*v/v*); FeMC6*a-PEG_4@AuNPs enzyme concentration 27.3

nM. For the experiments performed at variable ABTS, the H_2O_2 concentration was 100.0 mM. For the experiments performed at variable H_2O_2, the ABTS concentration was fixed at 5.0 mM.

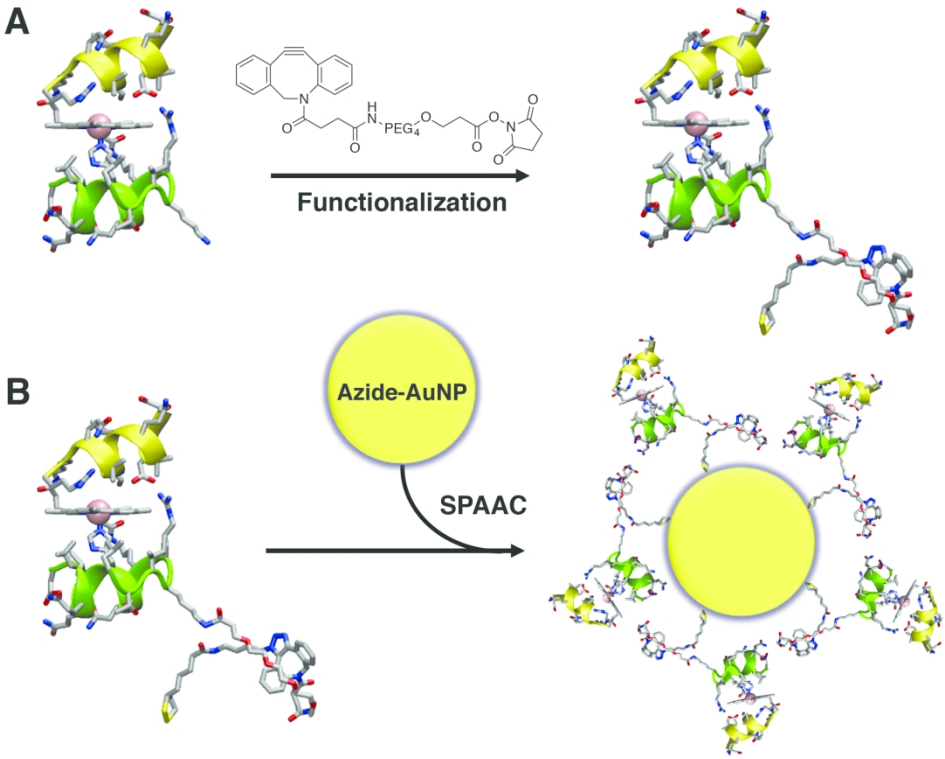

Figure 1. Clickable artificial peroxidase. A) Functionalization of FeMC6*a with the pegylated aza-dibenzocyclooctyne. B) Immobilization of FeMC6*a-PEG_4@DBCO on AuNPS, via SPAAC, to afford catalytically active nanomaterial.

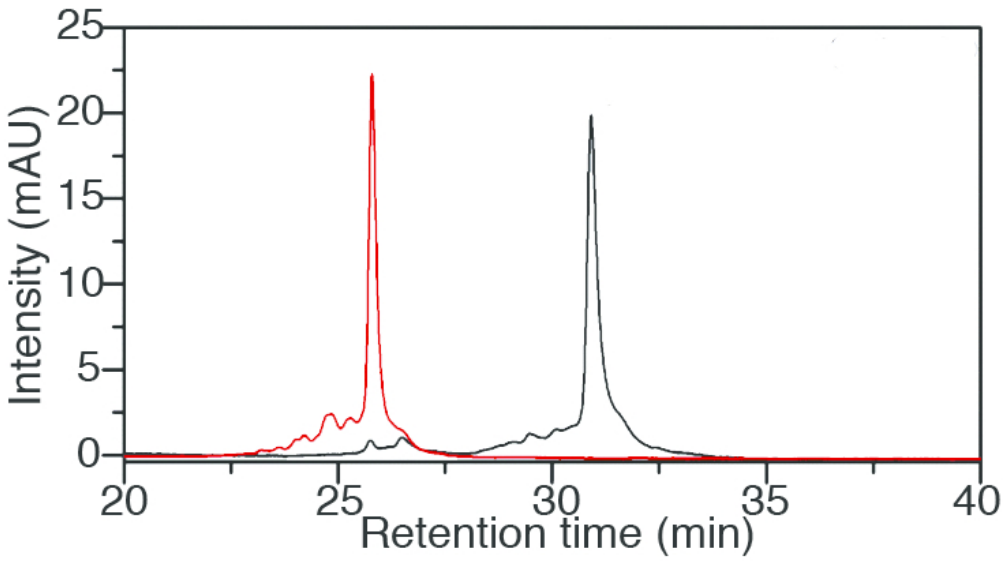

Figure 2. Comparison of the RP-HPLC chromatogram of FeMC6*a (red line) and of FeMC6*a-PEG_4@DBCO (black line).

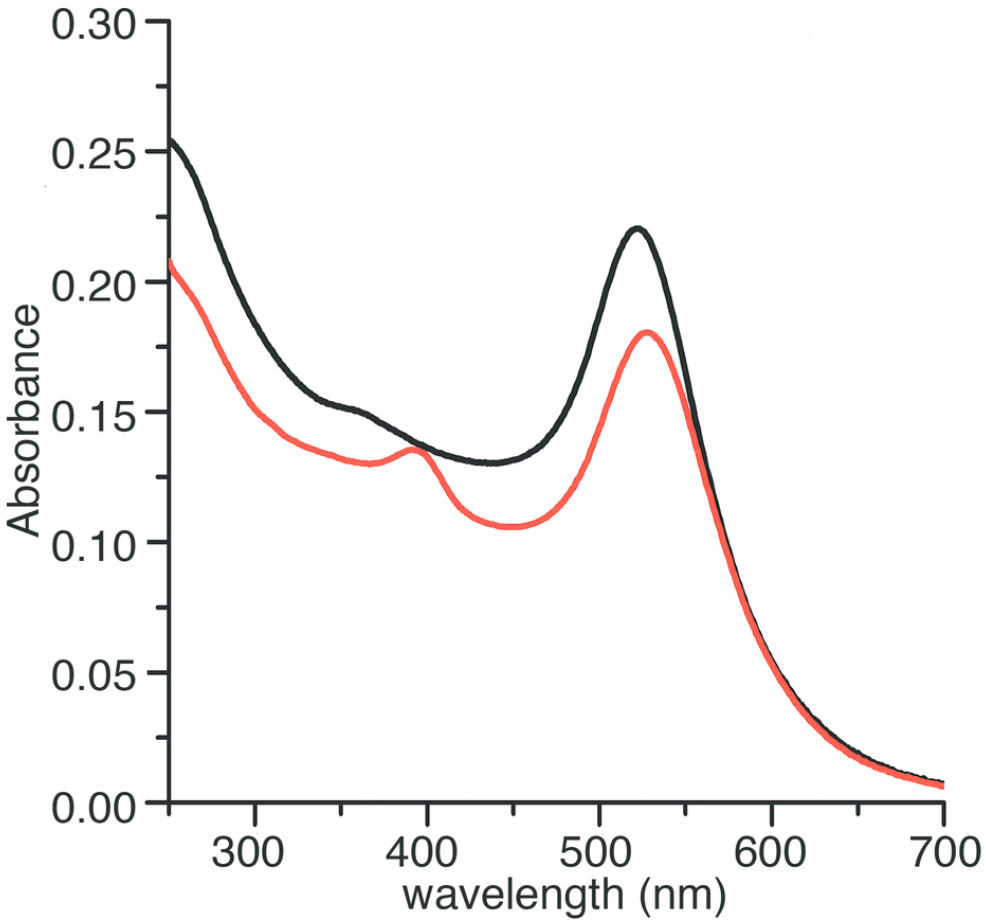

Figure 3. UV-Vis spectra of surface modified AuNPs: azide-AuNPs (red line, nanoparticle concentration 5.27 nM) and FeMC6*a-PEG_4@AuNPs (black line, nanoparticle concentration 4.31 nM).

80x80mm (300 x 300 DPI)

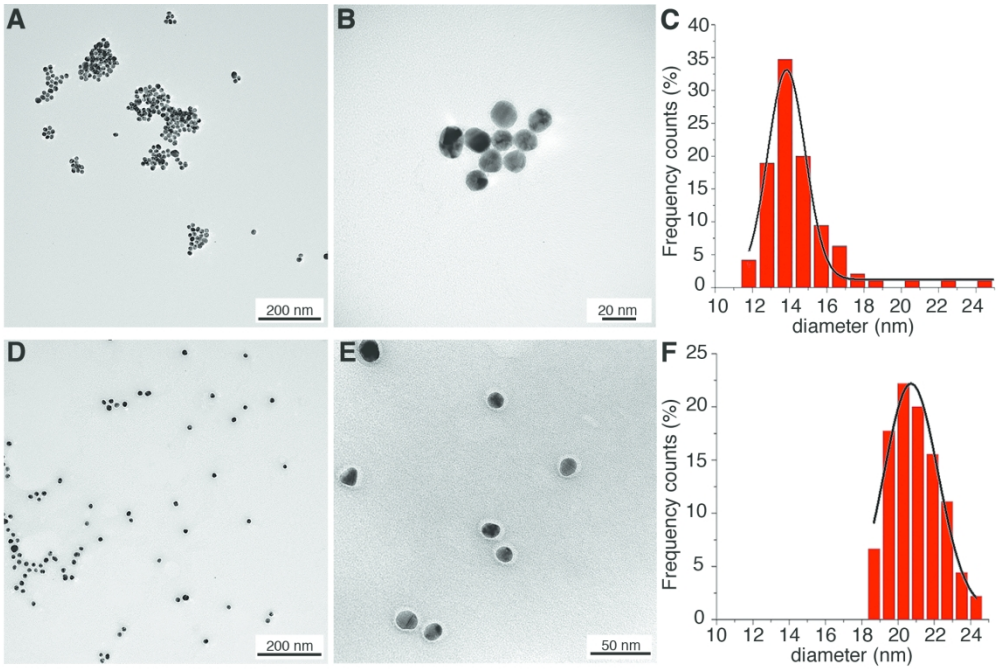

Figure 4. TEM images of the synthesized AuNPs, along with the corresponding size distribution histograms. A-C) Azide-AuNPs. D-F) FeMC6*a-PEG_4@AuNPs conjugate. The samples were stained with UranyLess before observation.

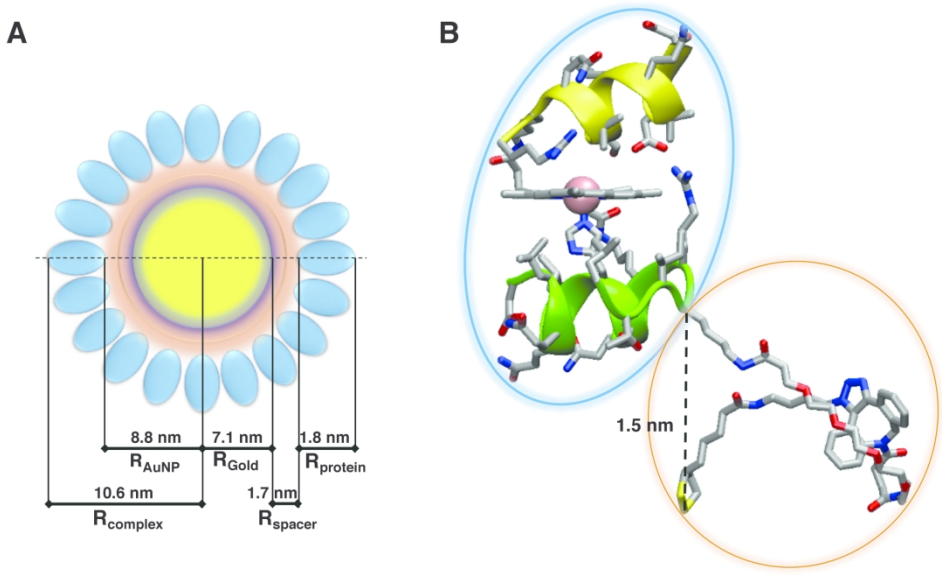

Figure 5. A) Schematic representation of the packing of FeMC6*a around a single AuNP. The dimensions of each conjugate component used for calculating Nmax (the maximum theoretical number of enzyme molecules that can be loaded on each spherical AuNP) are shown. B) FeMC6*a-PEG_4@LA molecular model. Backbone is represented as ribbon. (D) and (TD) chains are depicted in gold and in green, respectively. The distance between the sulfur atom of LA and the Cα atom of the Lys residue is also indicated. The model structure was generated with VMD [60].

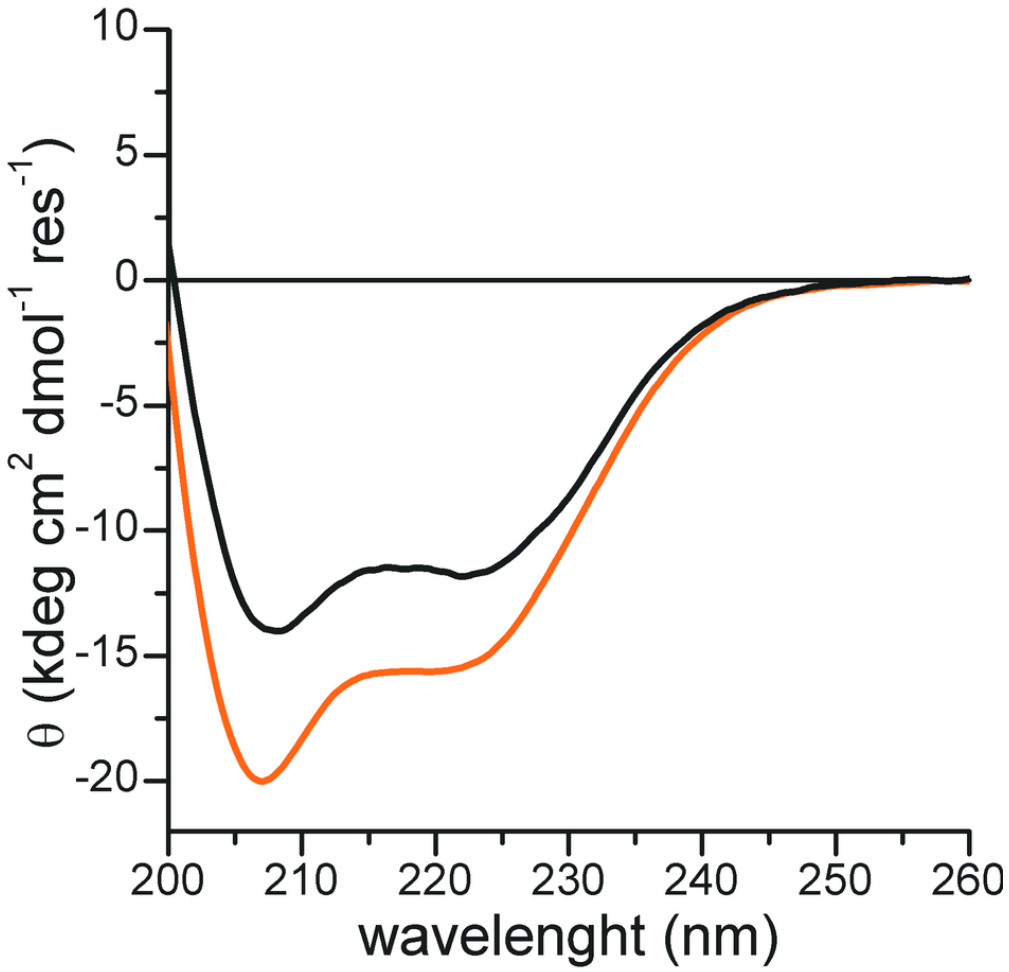

Figure 6. Superposition of the CD spectra of FeMC6*a-PEG$_4$@AuNPs and FeMC6*a (10 mM phosphate buffer (pH 6.5) 50% TFE (v/v).

79x79mm (300 x 300 DPI)

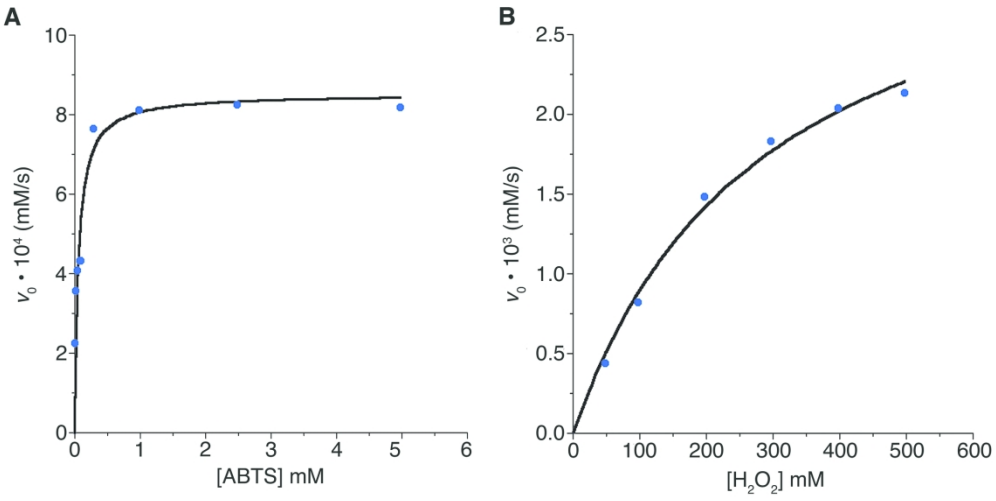

Figure 7. Peroxidase activity of FeMC6*a-PEG_4@AuNPs: A) initial rate dependence towards ABTS concentration; B) initial rate dependence towards H_2O_2 concentration. Reaction conditions were: 50.0 mM phosphate buffer pH 6.5 50% TFE (v/v); FeMC6*a-PEG_4@AuNPs enzyme concentration 27.3 nM. For the experiments performed at variable ABTS, the H_2O_2 concentration was 100.0 mM. For the experiments performed at variable H_2O_2, the ABTS concentration was fixed at 5.0 mM.

199x99mm (300 x 300 DPI)

Table 1. Catalytic parameters for FeMC6*a and FeMC6*a-PEG_4@AuNPS

Enzyme	K_m^{ABTS} (mM)	$K_m^{H_2O_2}$ (10^2 mM)	k_{cat} (10^2 s^{-1})	k_{cat}/K_m^{ABTS} (10^3 mM^{-1} s^{-1})	$k_{cat}/K_m^{H_2O_2}$ (mM^{-1} s^{-1})
FeMC6*a	0.09±1	4.4±0.5	58±3	64±8	13±2
FeMC6*a@AuNPs	0.193± 0.005	2.16±0.04	1.10±0.03	0.570± 0.001	0.509±0.003